Electrochemical Regeneration of Anthraquinones for Lifetime Extension in Flow Batteries

Yan Jing[†1], Evan Wenbo Zhao[†2,5], Marc-Antoni Goulet[†3,6], Meisam Bahari[3], Eric M. Fell[3], Shijian Jin[3], Ali Davoodi[3,4,7], Erlendur Jónsson[2], Min Wu[3], Clare Grey[2]✉, Roy G. Gordon[1,3]✉, Michael J. Aziz[3]✉

[1]Department of Chemistry and Chemical Biology, Harvard University, Cambridge, Massachusetts 02138, USA.
[2] Yusuf Hamied Department of Chemistry, University of Cambridge, Cambridge, UK.
[3]John A. Paulson School of Engineering and Applied Sciences, Harvard University, Cambridge, Massachusetts 02138, USA.
[4] Materials and Metallurgical Engineering Department, Faculty of Engineering, Ferdowsi University of Mashhad (FUM), Mashhad, 9177948974, Iran.
[5]Present address: Magnetic Resonance Research Center, Institute for Molecules and Materials, Radboud University Nijmegen, Nijmegen, Netherlands.
[6]Present address: Department of Chemical and Materials Engineering, Concordia University, Montreal, Quebec, Canada.
[7]Present address: Sichuan University-Pittsburgh Institute, Sichuan University, Chengdu, Sichuan Province, China.
[†]These authors contributed equally to this work.
✉e-mail: cpg27@cam.ac.uk; gordon@chemistry.harvard.edu; maziz@harvard.edu.

Abstract

Aqueous organic redox flow batteries (AORFBs) offer a safe and potentially inexpensive solution to the problem of storing massive amounts of electricity produced from intermittent renewables. However, molecular decomposition is the major barrier preventing AORFBs from being commercialized. Structural modifications can improve molecular stability at the expense of increased synthetic cost and molecular weight. Utilizing 2,6-dihydroxy-anthraquinone (DHAQ), without further structural modification, we demonstrate that electrochemical regeneration could be a viable route to achieve low-cost, long-lifetime AORFBs. *In situ (online)* NMR and EPR and complementary electrochemical analyses reveal that decomposition compounds *i.e.*, 2,6-dihydroxy-anthrone (DHA) and its tautomer, 2,6-dihydroxy-anthranol (DHAL), can be converted back to DHAQ in two steps: first $DHA(L)^{2-}$ are oxidized to the dimer $(DHA)_2^{4-}$ at –0.32 V vs. SHE by one-electron transfer; subsequently, the $(DHA)_2^{4-}$ is oxidized to $DHAQ^{2-}$ at +0.57 V vs. SHE by three-electron transfer. Electrochemical regeneration rejuvenates not only $DHAQ^{2-}$, but also the positive electrolyte – rebalancing the states of charge of both electrolytes without introducing extra ions. We demonstrate the repeated capacity recovery with DHAQ | potassium ferro-/ferricyanide flow battery in basic conditions, and show the approach is also effective for anthraquinone-2,7-disulfonate in acid. Electrochemical regeneration strategies may extend the useful lifetime of many water-soluble organic molecules with anthraquinone core structures in electrochemical cells.

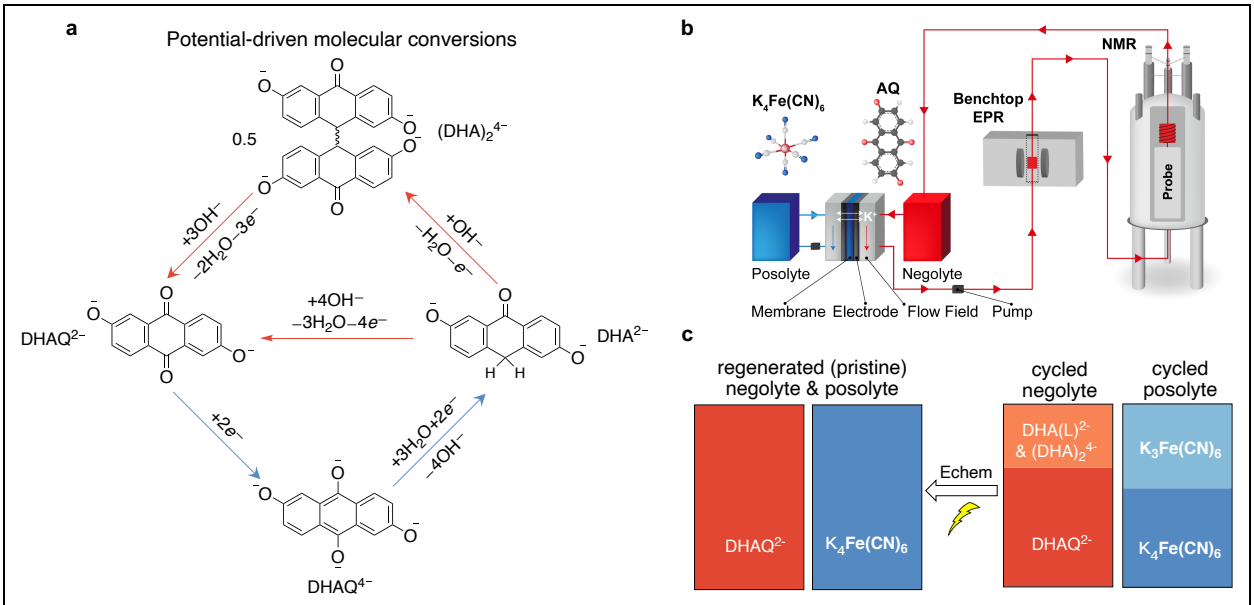

Scheme 1. Electrochemically rejuvenating a DHAQ | $Fe(CN)_6$ flow battery. a, Potential-driven DHAQ-related molecular conversions at pH 14. DHA^{2-} can tautomerize to $DHAL^{2-}$, which is shown in Figure 1c. **b**, *In situ* NMR and EPR metrologies used to monitor electrochemical conversions. **c**, A rejuvenated DHAQ flow cell resulting from the electrochemical regeneration. Negolyte denotes the negative electrolyte; posolyte denotes the positive electrolyte.

Organic molecules, when used for aqueous redox flow batteries, hold great promise to both lower the levelized costs of electricity storage significantly, while also outperforming their inorganic counterparts, being composed of earth abundant elements which possess considerable structural diversity and tunability.[1,2] However, the instability of organic molecules under the harsh electrochemical conditions found in aqueous organic redox flow batteries (AORFBs), is one the biggest obstacle for their commercialization.[3] While extremely stable redox organic molecules have been synthesized, this comes at the expense of increased synthetic cost and molecular weight.[4-9]

2,6-Dihydroxyanthraquinone (DHAQ), while an inexpensive molecule (estimated cost: \$4.02/kg, \$23.70/kAh),[10] shows a fast temporal fade rate due to the instability of the reduced DHAQ ($DHAQ^{4-}$), which reacts to form redox-inactive 2,6-dihydroxyanthrone (DHA) along with its tautomer, 2,6-dihydroxyanthranol (DHAL).[11,12] Goulet and Tong *et al.*, however, reduced the reaction rate by restricting the negative electrolyte (negolyte) state of charge (SOC) and converted a substantial amount of the $DHA(L)^{2-}$ back to $DHAQ^{2-}$ by aeration of the negolyte, thereby extending the overall lifetime of the battery.[11] The $DHAQ^{4-}$ can also be electrochemically reduced to form $DHA(L)^{2-}$,[12,13] which can be subsequently electrochemically oxidized to the dimer $(DHA)_2^{4-}$.[11] Since the direct electrosynthesis of the water-soluble anthraquinones from their anthracene precursors has already been demonstrated by some of us, via a multiple-electron transfer processes,[14] we set out to exploit much of the above insight to study the viability of electrochemically regenerating DHAQ from the redox-inactive (reduced) compounds. *In situ* NMR and EPR metrologies are used to observe the stepwise conversions in real time, *i.e.*, $DHAQ^{2-}$ to $DHAQ^{4-}$, to $DHA(L)^{2-}$, then to its dimer $(DHA)_2^{4-}$, and finally back to $DHAQ^{2-}$, by adjusting cell voltages "on the fly" (Scheme 1). The conversions from $DHA(L)^{2-}$ to $DHAQ^{2-}$ are further confirmed by a $DHA(L)^{2-}$ | $[Fe(CN)_6]^{3-/4-}$ flow cell, and corresponding oxidation potentials are determined by an embedded reference electrode. In combination with the demonstrated electrochemical reduction, this study exhibits the full loop of DHAQ electrochemical molecular conversions and demonstrates the electrochemical regeneration of anthraquinone redox flow batteries.

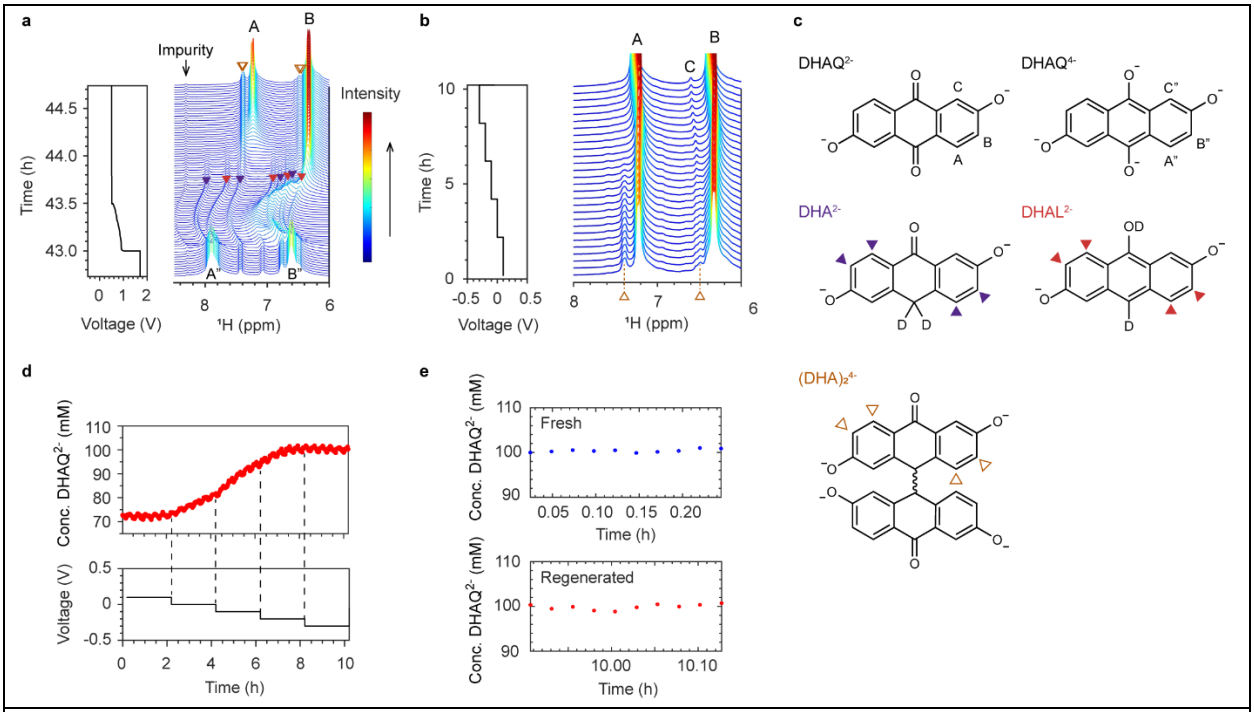

Figure 1. ***In situ*** **^{1}H NMR spectra acquired during the electrochemical cycling. a**, Voltage of the battery composed of 25 mL 100 mM DHAQ as the negolyte and a mixture of 50 mL 200 mM $K_4[Fe(CN)_6]$ and 100 mM $K_3[Fe(CN)_6]$ as the positive electrolyte (posolyte). 1.2 M and 1 M KOH dissolved in D_2O were used as solvents for the negolyte and posolyte, respectively. Nafion 117 was used as the membrane. The voltage was held at 1.7 V, then a constant current of –30 mA/cm^2 was applied, followed by a voltage hold at 0.5 V. The full voltage profile for the electrochemical cycling experiment is shown in Figure S1. The corresponding *in situ* ^{1}H NMR spectra of the negolyte in the aromatic region is shown on the right. The color bar (right) indicates the intensity of resonances. The solid purple, red and hollow brown triangles highlight the signals of the decomposition products, DHA^{2-}, $DHAL^{2-}$ and $(DHA)_2^{4-}$ anions, respectively. The proton resonances are labelled A and B for DHAQ, with double-prime labels indicating the same protons in the singlely and doubly reduced anions, respectively. **b**, *In situ* ^{1}H NMR spectra acquired during a stepped voltage-hold experiment. **c**, Molecular structures of the $DHAQ^{2-}$, $DHAQ^{4-}$, DHA^{2-}, $DHAL^{2-}$ or $(DHA)_2^{4-}$ anions. **d**, Concentration of $DHAQ^{2-}$ anions (top) and the voltage of the battery (bottom) as a function of time during the stepped voltage-hold experiment. **e**,

Concentrations of $DHAQ^{2-}$ anions in a fresh uncycled negolyte solution (top) and at the end of the voltage hold at −0.3 V (bottom). The concentrations were calculated from the intensities of signal A.

The evolution of *in situ* ^{1}H NMR spectra of 100 mM DHAQ during the discharge phase of an electrochemical cycle is shown in Figure 1a. Following an initial charge at 30 mA/cm^2, the voltage of the battery was held at 1.7 V for 42 hours. The ^{1}H NMR signals A" and B" of the $DHAQ^{4-}$ anions are clearly visible along with weaker signals from $DHA(L)^{2-}$ at 6.49, 6.57, 6.77, 7.08, 7.43, 7.82 and 7.95 ppm. The cell was then discharged by a constant current of −30 mA/cm^2, the voltage decreasing rapidly to 0.9 V and then dropping more gradually to a cut-off voltage of 0.5 V. This was followed by a voltage hold at 0.5 V for 7.4 hours. Note that a second voltage plateau at 0.7 V during discharge, as previously reported,[13] was not observed due to the high overpotential caused by the thick Nafion 117 membrane used in this experiment. During discharge, the fast electron transfer between $DHAQ^{3-\bullet}$ and $DHAQ^{4-}$ anions causes broadening of peaks A" and B", allowing the DHA^{2-} and $DHAL^{2-}$ signals (marked with solid purple and red triangles) to be seen more clearly as they remain unaffected by this broadening mechanism, consistent with our earlier studies.[12,13] The shift of all of these signals is caused by the change of the bulk magnetization of electrolyte solution as $DHAQ^{3-\bullet}$ anions were produced from $DHAQ^{4-}$ oxidation and then further oxidized to $DHAQ^{2-}$. During the voltage hold at 0.5 V, the $DHAQ^{2-}$ A and B peaks, and new signals at 6.36, 6.41, 7.40 and 7.41 ppm (marked with hollow brown triangles) grow in, accompanied by the decrease of signal intensities of $DHA(L)^{2-}$. The new peaks are assigned to $(DHA)_2^{4-}$ on the basis of an *in situ* 2D ^{1}H homonuclear correlation spectrum (COSY), as shown in Figure S2. Therefore, at 0.5 V (vs. the $K_4[Fe(CN)_6]$/ $K_3[Fe(CN)_6]$ couple) $DHA(L)^{2-}$ can be electrochemically oxidized to $(DHA)_2^{4-}$.

To test whether $(DHA)_2^{4-}$ can be oxidized further, the voltage of the battery was decreased from 0.1 V to −0.3 V, in steps of 0.1 V, holding for 2 hours at each voltage step. The corresponding *in situ* ^{1}H NMR spectra are shown in Figure 1b. The intensity of the $(DHA)_2^{4-}$ dimer signals (marked with hollow brown triangles) start to decrease at 0.1 V with the rate of intensity drop increasing as the voltage is held at a more negative vaule, the signals disappearing completely at −0.2 V (Figure S2e), accompanied by the increase of signal intensities of $DHAQ^{2-}$. This observation suggests that $(DHA)_2^{4-}$ has been electrochemically oxidized to $DHAQ^{2-}$, following our proposed molecular conversion (Scheme 1a). The shift of signals A, B and C at −0.3 V was caused by the change in the bulk magnetization of electrolyte solution, induced by the oxidation of the ferrocyanide ions that have crossed the membrane into the negolyte.

The concentration of $DHAQ^{2-}$ as a function of voltage has been quantified (Figure 1d) and remains at 72 mM at 0.1 V, starting to increase to 80 mM, 95 mM and 100 mM at 0 V, −0.1 V and −0.2 V, respectively. A comparison of the initial concentration of $DHAQ^{2-}$ (*i.e.*, 100.4 mM ± 0.25 mM) with the concentration after electrochemical regeneration (*i.e.*, 99.9 mM ± 0.44 mM) is shown in Figure 1e. A volumetric loss of 2.0 mL from the negolyte solution (DHAQ) was measured at the end of the experiment. The loss could be caused by water crossover from the negolyte to the posolyte and water splitting in the negolyte. Taking into account this volumetric loss, a lower limit of concentration for recovered $DHAQ^{2-}$ is 91.9 mM. A second experiment with voltage holds down to −0.6 V has also shown a substantial regeneration of $DHAQ^{2-}$ anions (Figure S3). Furthermore, the degradation products DHA^{2-} and $DHAL^{2-}$ anions were produced again when the voltage was increased to 1.7 V (Figure S3), demonstrating the circularity of the electrochemical reactions from $DHAQ^{2-}$ to $DHA(L)^{2-}$, to $(DHA)_2^{4-}$ and back to $DHAQ^{2-}$ at different potentials, as illustrated in Scheme 1a. Note that no degradation products were detected at the end of the regeneration step within the detection limit of 0.4 mM (see Pseudo-2D NMR in *Methods* for details on the detection limit) for the *in situ* NMR method, suggesting that if any degradation product persists, it is NMR-silent or below the instrument detection limit. This possibility will be discussed further in the following text.

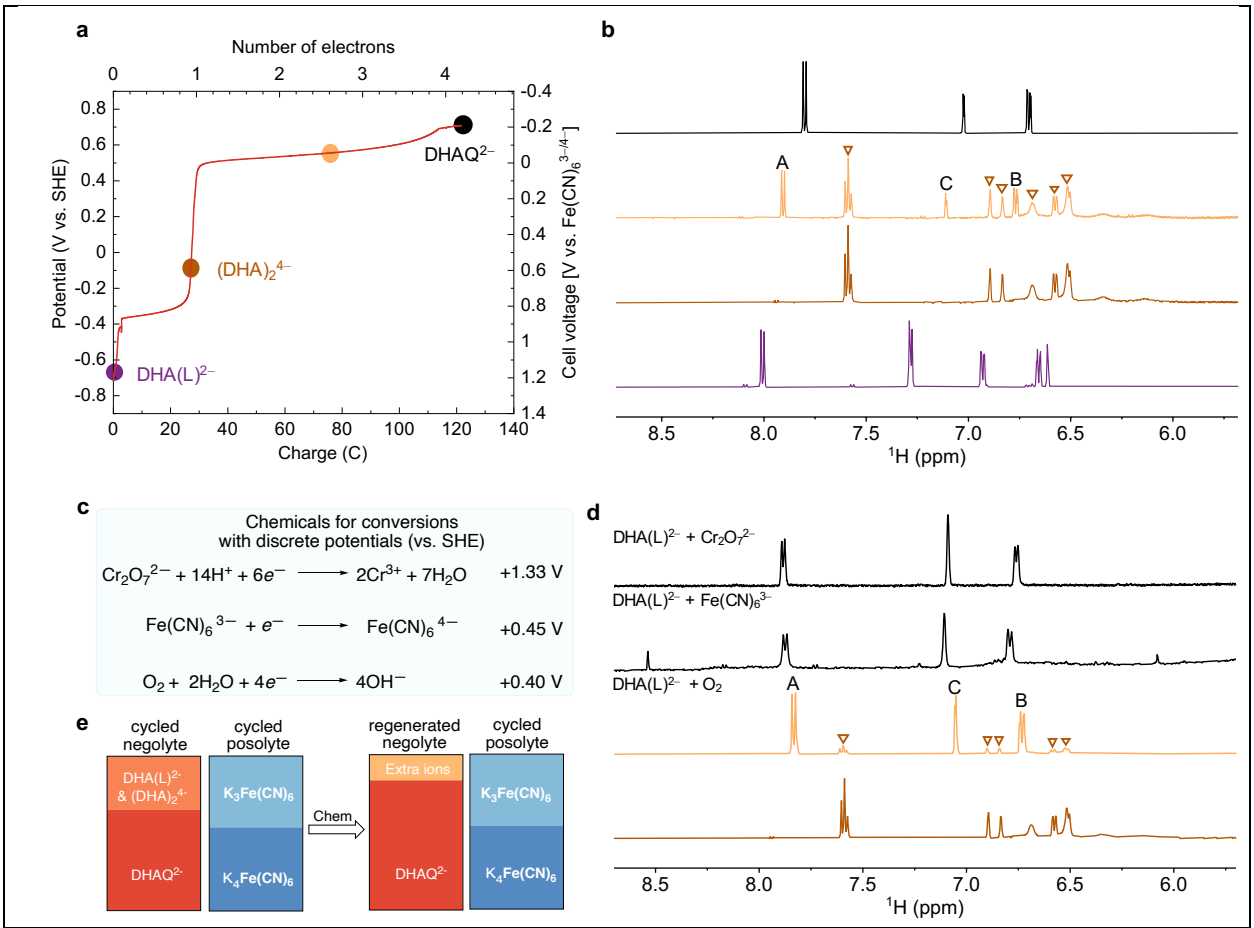

Figure 2. Electrochemical vs. chemical oxidations of DHA(L)$^{2-}$. a, Voltage profile of the DHA(L)$^{2-}$ | [Fe(CN)$_6$]$^{3-/4-}$ flow cell with an embedded Hg/HgO (1 M KOH) reference electrode. The battery is composed of 6 mL 50 mM DHA(L)$^{2-}$ as the negolyte and a mixture of 120 mL 40 mM K_4[Fe(CN)$_6$] and 20 mM K_3[Fe(CN)$_6$] as the posolyte. A galvanostatic discharge at 40 mA/cm^2 with a potential hold at –0.2 V vs. Fe(CN)$_6$ with current cutoffs of 1 mA/cm^2 was performed. The circles indicate points where aliquots were extracted for *ex situ* analysis **b**, *Ex situ* ^{1}H NMR spectra acquired at different potentials of DHA(L)$^{2-}$ negolytes taken from the DHA(L)$^{2-}$ | Fe(CN)$_6$ flow cell. Bottom to top: aliquot taken from the DHA(L)$^{2-}$ negolyte before any potential is applied (purple) and aliquot taken when the potential of the negolyte was at –0.1 V (brown), +0.5 V (yellow) and +0.65 V (black). The colour scheme corresponds to that used for the circles in (a); the hollow brown trianges correspond to the peaks from the (DHA)$_2^{4-}$; the A, B and C indicate the DHAQ^{2-} resonances in Figure 1c. **c**, Chemicals used for DHA(L) oxidations and their reduction potentials. **d**, ^{1}H NMR spectra of (DHA)$_2^{4-}$ and aliquots (0.1 M, 100 uL/each) taken after the different chemical reactions. Bottom to top: aliquot from (DHA)$_2^{4-}$ serves as a control (brown); aliquot from DHA(L)$^{2-}$ sample exposed to oxygen (yellow); aliquot from DHA(L)$^{2-}$ sample mixed with five equivalents of ferricyanide (black), (where the peak at 8.52 ppm corresponds to the partially protonated hydroxyl groups in DHAQ); aliquot from DHA(L)$^{2-}$ sample mixed with five equivalents of $K_2Cr_2O_7$ in acid, filtered to collect the precipitates and remove the Cr$^{3+/6+}$ solution, then re-dissolved the precipitates in base (black). **e**, Schematic of the rejuvenated DHAQ^{2-} flow cell that results from chemical regeneration. Extra ions such as Cr^{3+}, Fe(CN)$_6^{4-}$, or OH$^-$ will be inevitably introduced to the negolyte because of the use of chemicals for conversions. The small variation of DHAQ^{2-} chemical shifts between different samples are due to the slight differences in pH.

To explore the regeneration of DHAQ^{2-}, as revealed by the *in situ* ^{1}H NMR spectra, further we synthesized DHA(L) [11] and built a separate DHA(L)$^{2-}$ | [Fe(CN)$_6$]$^{3-/4-}$ flow cell. By applying constant current to the negolyte vs. [Fe(CN)$_6$]$^{3-/4-}$, we first converted DHA(L)$^{2-}$ to (DHA)$_2^{4-}$ by one-electron transfer, then (DHA)$_2^{4-}$ to pure DHAQ^{2-} by three-electron transfer, with a close to quantitative yield (>95%) (Figure 2a). The *ex situ* ^{1}H NMR spectra (Figure 2b) show that the peaks from DHA(L)$^{2-}$ fully disappear and the peaks from (DHA)$_2^{4-}$ dominate at –0.1 V; the peaks from (DHA)$_2^{4-}$ and DHAQ^{2-} coexist at 0.5 V; eventually, the peaks from DHAQ^{2-} dominate at 0.65 V. This potential-driven stepwise conversions corroborate the *in situ* ^{1}H NMR guided result (Figure 1d, 1e), indicating that electrochemical oxidation is indeed feasible.

Although chemical oxidation of $DHA(L)^{2-}$ by oxygen recovers a substantial amount of $DHAQ^{2-}$, some $(DHA)_2^{4-}$ remains due to the proximity of the dimer (0.57 V vs. SHE, Figure S4b) and oxygen redox potentials (0.40 V vs. SHE) (Figure 2c). By contrast, other chemical oxidants with higher oxidation potentials such as $Cr_2O_7^{2-}$ under acidic conditions (Figure 2d), or ferricyanide in basic condition fully convert $DHA(L)^{2-}$ into $DHAQ^{2-}$ (Figure S10). However, they inevitably introduce extra ions to the electrolyte, leading to system imbalance.

As displayed in Figure 2 and with other experiments involving pure $DHA(L)^{2-}$ (Figure S4), we demonstrate that conversion of $DHA(L)^{2-}$ and $(DHA)_2^{4-}$ back to $DHAQ^{2-}$ is possible by electrochemical oxidation. This recovery method is greatly advantageous over chemical oxidation for three key reasons: 1. The disproportionation reaction, which creates $DHA(L)^{2-}$, also unbalances the SOC and changes the pH of the electrolytes. Electrochemical regeneration of $DHAQ^{2-}$ rebalances the SOC and restores the pH, closing the cycle and bringing the cell back to its initial conditions (Scheme 1c). In contrast, chemical oxidation further alters the chemical composition and pH of the electrolyte solution (Figure 2c, 2e). 2. Electrochemical regeneration avoids the costs associated with periodically adding chemical oxidants to the negolyte. 3. Electrochemical regeneration does not add solute to the negolyte that might eventually cause precipitation of active species or cross the membrane and interact badly with posolyte species.

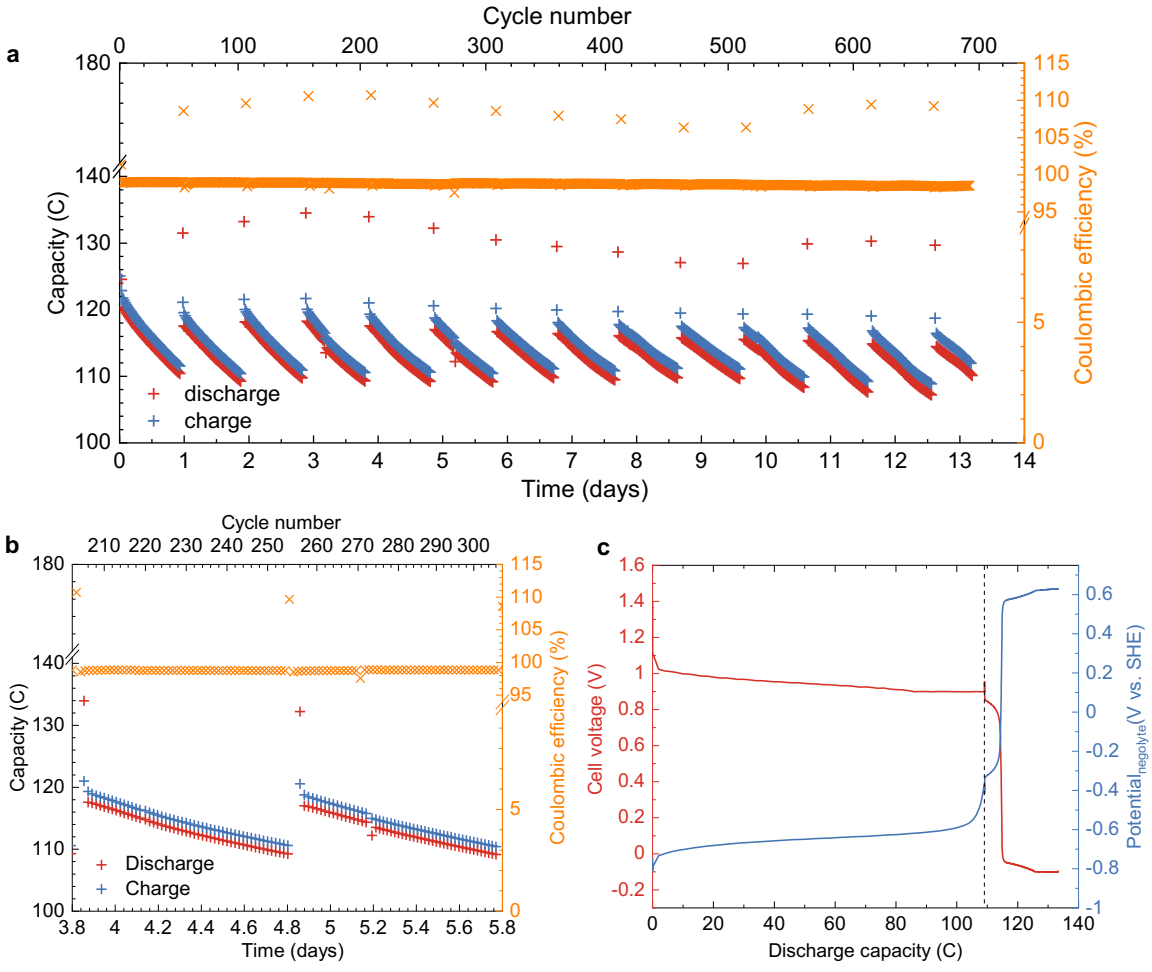

Figure 3. Long-term cycling of $DHAQ^{2-/4-}$ | $[Fe(CN)_6]^{3-/4-}$ flow battery with capacity recovery by electrochemical regeneration of the negolyte. a, Repeated application of electrochemical regeneration of negolyte in a flow battery composed of 6.5 mL 100 mM $DHAQ^{2-}$ as the negolyte and a mixture of 35 mL 60 mM $K_4[Fe(CN)_6]$ and 30 mM $K_3[Fe(CN)_6]$ as the posolyte. Galvanostatic cycling at 40 mA/cm^2 with potential holds at 0.9 and 1.4 V during normal cycles with current cutoffs of 1 and 2 mA/cm^2 for discharge and charge, respectively. Every 50 cycles an additional discharge step at 2 mA/cm^2 until the potential reaches –0.1 V and a further hold until current decreases to 0.4 mA/cm^2 was performed b, Highlighted example of electrochemical regeneration of negolyte on day-4.8 during discharge. Red and

blue "+" marks represent discharge capacity and charge capacity, respectively. Orange "×" marks represent coulombic efficiency. c, Example of a full cell and negolyte potential during the additional discharge step down to –0.1 V. The cell voltage and potential changes during the standard cycling protocol are shown to the left of the dashed line, whereas to the right are those during the conversions of $DHA(L)^{2-}$ to $(DHA)_2^{4-}$ and of $(DHA)_2^{4-}$ to $DHAQ^{2-}$.

To demonstrate the effectiveness and sustainability of the electrochemical regeneration strategy, a $DHAQ^{2-}$ | $[Fe(CN)_6]^{3-/4-}$ full cell was cycled with an additional discharge step down to –0.1 V every 50 cycles. During each of these additional discharge treatments, the potentials of both the negolyte and the full cell demonstrate two additional oxidation plateaus, which correspond to the dimerization of $DHA(L)^{2-}$ and the subsequent oxidation of the $(DHA)_2^{4-}$ back to $DHAQ^{2-}$. The capacity measured during the first oxidation plateau (at around –0.3 V vs. SHE) is almost one-third the capacity measured during the second plateau (at around 0.6 V vs. SHE). This observation, further confirmed by volumetrically unbalanced, compositionally symmetric cell testing (Figure S5), is consistent with the electrochemical oxidation of $DHA(L)^{2-}$ in Figure 2a and the proposed reactions in Scheme 1a, as the oxidation of $DHA(L)^{2-}$ involves one electron while the dimer loses three electrons per molecule of $DHA(L)^{2-}$ to form $DHAQ^{2-}$. Figure 3 shows significant recovery after each of these treatments in agreement with the evidence from *in situ* NMR of accelerated decomposition and recovery under similar conditions. In all cases, the ratio of capacity recovery to capacity lost in the preceding 50 cycles always exceeds 93% except for the first case (71.0%) and averages to 94.7%. Repeated experiments show similar behavior with unusually high recovery occurring following a segment with a low recovery ratio (Figure S6), which suggests that any unconverted DHA will remain in the electrolyte for subsequent regeneration.

The average recovery in Figure 3 leads to an overall residual fade rate of 0.38%/day, which is an order of magnitude improvement over the initial instantaneous fade rate of 6.45%/day in this experiment. Additional cell cycling experiments also suggest that the effectiveness of the regeneration treatment is unrelated to the amount of $DHA(L)^{2-}$ formed (Figure S9c). This implies that the residual capacity fade of the battery is no longer related to the previously published anthrone-related capacity fade mechanism.[11] By addressing this degradation mechanism with electrochemical regeneration, it is no longer necessary to perform SOC-restricted cycling, thereby enabling the utilization of more of the negolyte – with a corresponding reduction in system cost. Although long-term cycling and recovery experiments such as the one shown in Figure 3a have not demonstrated the complete recovery of battery capacity, extensive characterization of cycled negolytes with substantial capacity loss has not indicated any appreciable decomposition products after additional discharge at –0.1 V (Figure S7). In addition, concentration measurements by cyclic voltammetry and NMR of the negolyte suggest that the concentration of $DHAQ^{2-}$ has not been lost (Figure S7), although these may be overestimated by water splitting in the negolyte and water crossover from negolyte to posolyte during the electrochemical oxidations. Preliminary studies suggest that this secondary capacity fade may be due in part to the open circuit voltage (OCV) drift of the electrolytes over cycling (Figure S8). However, capacity fade due to additional molecular decompositions including fragmentation, polymerization, or $DHAQ^{2-}$ tautomerization,[15] has not been entirely excluded yet. Further investigation into these secondary capacity fade mechanisms is ongoing.

The high fade rate of $DHAQ^{2-/4-}$ makes it particularly suitable for demonstrating the effectiveness of the electrochemical regeneration method described in this study; however this method would also be applicable to other anthraquinone negolytes with low (0.02–0.1%/day) or moderate (0.1–1%/day) fade rates[3] which also suffer from the same anthrone disproportionation mechanism. One such example is anthraquinone-2,7-disulfonic acid (AQDS)[10,16] that has a much lower fade rate of 0.1%/day in acid at room temperature,[17] but decomposes to anthrone (anthranol)-2,7-disulfonic acid (ADS) over cycling (Figure S12).[18] Our preliminary results confirm that ADS (both pure ADS and produced by cycling AQDS) can be chemically and electrochemically converted to AQDS (Figure S13, S14, S15). Thus this approach should reduce the overall fade rate of these negolytes, potentially enabling them to reach electrolyte lifetimes comparable to more recent studies utilising more complex and costly reactants.[5-7] More generally, we expect the same anthrone-based capacity fade mechanism to be present in even those ultra long lifetime anthraquinone electrolytes and, as such, could also be reversed by the electrochemical regeneration method demonstrated in this work.

Conclusion

This work demonstrates the power of *in situ* ^1H NMR and EPR metrologies to reveal and quantify the reactions occurring in electrochemical flow cells. We have shown that the decomposition compounds $DHA(L)^{2-}$ in cycled DHAQ electrolytes can be converted back to $DHAQ^{2-}$, validating our proposed mechanism. Mechanistic study indicates that the conversion proceeds in two steps: first, $DHA(L)^{2-}$ is oxidized to $(DHA)_2^{4-}$ with one-electron transfer at –0.32 V vs. SHE; second, $(DHA)_2^{4-}$ is oxidized to $DHAQ^{2-}$ with three-electron transfer at +0.57 V vs. SHE, with the two steps consuming one and three hydroxide ions, respectively. These oxidative interventions close the loop of DHAQ-related potential-driven molecular conversions. We utilize them to repeatedly demonstrate the electrochemical regeneration of the DHAQ | $Fe(CN)_6$ alkaline flow battery. Electrochemical regeneration not only rejuvenates the negolyte, but also rebalances the state of charge of both

electrolytes. AQDS preliminary studies further show both the feasibility of electrochemical regeneration at pH 0 and that this is not a peculiar feature of DHAQ. The electrochemical regeneration method should extend to other anthraquinones susceptible to anthrone formation; similar strategies may also be applicable for other redox-active organic molecules. Electrochemical regeneration could permit redox-active organic molecules to reach the combination of performance, cost, and lifetime necessary for AORFBs to become an attractive solution to the intermittent renewable electricity storage problem.

Acknowledgments

Research at Harvard was supported by the U.S. National Science Foundation through grant CBET-1914543 and by U.S. DOE award DE-AC05-76RL01830 through PNNL subcontract 535264. Research at University of Cambridge was supported by Centre of Advanced Materials for Integrated Energy Systems (CAM-IES), via EPSRC grant no. EP/P007767/1 and Shell. E.W.Z acknowledges the STFC Futures Early Career Award, grant no. ST/R006873/1. We acknowledge P. A. A. Klusener from Shell for useful discussions.

Author contributions

M.A.J., R.G.G., C.P.G. supervised the project. Y.J., E.W.Z., M.-A.G., M.A.J., R.G.G., and C.P.G. conceived the idea. Y.J., E.W.Z., and M.-A.G. designed the experiment. E.W.Z. performed the *in situ* NMR and EPR experiments and analysis. Y.J. performed the *ex situ* NMR experiments and analysis. M.-A.G., M.B., E.M.F., and Y.J. performed DHA(L), ADS elctrochemical oxidations, DHAQ, AQDS cell cyclings. M.B. performed three-electrode cell tests. M.-A.G., S.J. and Y.J. performed postmortem CV, NMR, LC–MS experiments and analysis. A.D. performed the DHAQ cell cycling with periodic aeration. M.W. and Y.J. synthesized DHA(L), ADS, respectively. All authors contributed to the discussion of the project. Y.J., E.W.Z, M.-A.G., M.A.J., C.P.G. worte the manuscript with input from all co-authors.

Experiments and methods

In situ NMR and EPR study

Flow cell assembly

The cell assembly was described in detail in our previous work.[12] Briefly, graphite flow plates with serpentine flow patterns were used for both electrodes. Each electrode is composed 4.6 mm carbon felt (SGL) with a 5 cm^2 active area, which was used without further treatment. Either Nafion 117 or 212 were used as the ion transport membranes (see Figure caption for the specific one is used for the experiment). Pretreatment of the Nafion 117 membranes was performed by first heating the membrane in 80 °C deionized water for 20 min and then soaking it in 5% hydrogen peroxide solution for 35 min. The flow rate was set at 13.6 mL/min.

Electrochemical cycling in Figure S1a and S1b

The cell was charged by a constant current of 30 mA/cm^2, followed by a voltage hold at 1.7 V for 42 hours. It was then discharged by a constant current of −30 mA/cm^2, followed by a voltage hold at 0.5 V for 7.4 hours, at 0.2 V for 1 hour and −0.1 for 0.6 hour. After the voltage hold, the battery was set in a rest state for 36.8 hours.

Following the rest, the voltage was decreased from 0.1 V to −0.3 V, in steps of 0.1 V, holding for 2 hours at each voltage step. Then the battery was charged by a constant current of 20 mA/cm^2 followed by a voltage hold at 1.7 V for 1 hour, discharged by a constant current of −20 mA/cm^2 followed by a voltage hold at 0.6 V for 1 hour. The charge-discharge cycles were repeated three times.

The volumetric loss of electrolyte solution was measured by marking the liquid level in the electrolyte reservoir (a glass cylindrical tube with inlet and outlet) before the cycling and marking the liquid level after the cycling. The volume difference between these two marks were measured, and is equal to the volumetric loss.

Online NMR and EPR setup

The setup has been described in detail in our previous publication.[12] Briefly, the setup consists of a flow cell system, a bench-top EPR (MS5000, Magnettech) and an NMR (300 MHz, Bruker) spectrometer. The electrolyte solution is pumped through the flow cell, then flowed through the EPR and NMR magnets, finally back to the electrolyte reservoir. The direction of flow is from the bottom to the top through both magnets. 1/16 inch PFA tubes are used to connect the electrolyte reservoir, the battery, the EPR and NMR sampling tubes. A flow-through NMR sampling tube with 10 mm in O.D. was used. To minimize heating of the aqueous solution by microwave irradiation, a flat EPR cell (E4503, Magnettech) is used. The cell is orientated in the resonator such that the strength of the magnetic field is maximized, and the strength of the electric field is minimized across the sample. The time it takes for a round-trip from and back to the electrolyte reservoir is 64 s at a flow rate of 13.6 cm^3 min^{-1}. The time it takes for the electrolyte solution to travel from the electrolyte reservoir to the battery is 3 s, from the battery to the EPR detection region is 3 s, from the EPR to the NMR detection region is 29 s, and from the NMR detection regions back to the electrolyte reservoir is 29 s, respectively. Data reported in Figure S3 were acquired by the

coupled *online* NMR and EPR method. Since no EPR-active degradation products were detected, the rest of the *in situ* data were acquired by *online* NMR only.

Pseudo-2D NMR

Pseudo-2D NMR experiments were performed on flowing electrolyte solution by direct excitation with a 90° radio-frequency pulse. Each NMR spectrum is acquired by collecting 8 free induction decays (FIDs) with a recycle delay of 10 s. The pulse width for a 90° pulse was 29 μs at 60 W. All spectra were referenced to the water chemical shift at 4.79 ppm before cell cycling starts.

For the calculations of DHAQ concentration, the pseudo-2D NMR spectra were first baseline-corrected by a 4th order polynomial function. The resonance of DHAQ proton A was used for the calculation of DHAQ concentration. The signal integral of resonance A before the start of electrochemical cycling is normalized to 100 mM. The signal-to-noise (SNR) ratio for resonance A at 100 mM is 696.7. A SNR of 3 sets the detection limit, the detection limit for the in situ NMR using the current parameters is therefore 0.4 mM.

2D COSY NMR

Two-dimensional homonuclear correlation spectroscopy (COSY) NMR experiments were performed on the electrolyte solution with $DHA(L)^{2-}$ during flow and on the electrolyte solution with $(DHA)_2^{4-}$ when the flow is stopped. A pulsed field gradient (PFG)-enhanced double quantum filter COSY pulse sequences was applied.[19] For the spectrum acquired of $DHA(L)^{2-}$ (Figure S2c), the second dimension was constructed using 512 increments spanning 10 ppm. The recycle delay was 2 s and number of scans for each increment was 4. For the spectrum acquired on $(DHA)_2^{4-}$ (Figure S2d), the second dimension was constructed using 1024 increments spanning 10 ppm. The recycle delay was 2 s and number of scans for each increment was 16.

EPR parameters

For the EPR experiments, the magnetic field was swept from 336.5 mT to 339 mT. P was 0.5 mW and B_m was 0.001 mT. The acquisition time per EPR spectrum is 88 s, with a scanning time of 60 s, a coupling time of 20 s (time for automatic tuning) and a delay time of 8 s.

Electrochemical characterizations

Cyclic voltammetry measurements

Glassy carbon was used as the working electrode for all three-electrode CV tests with a 5 mm diameter glassy carbon working electrode, an Ag/AgCl reference electrode (BASi, pre-soaked in 3 M NaCl solution), and a graphite counter electrode. All cyclic voltammetry, linear sweep voltammetry, and chronoamperometry measurements were conducted on Gamry Instruments and CHI Instrument electrochemical analyzers.

Flow cell setup

Flow cell experiments were constructed with cell hardware from Fuel Cell Tech (Albuquerque, NM) or in-house cell with end plates made from PVC. Both designs were assembled into a zero-gap flow cell configuration using either pyrosealed POCO graphite flow plates or resin-impregnated carbon flow plates from MWI with identical interdigitated flow fields. Each electrode was composed of 1 or 2 layers of Zoltek PXFB carbon cloth with a 5 cm^2 geometric surface area. Nafion 117 membranes pre-soaked in 1 M KOH for at least 24 hours were used in all cell cycling tests.

In order to independently track the potential of the negative electrode as presented in Figure 3, a Hg/HgO reference electrode (BASi, with an internal electrolyte of 1 M KOH) was positioned externally on the inlet of the negolyte stream.

Materials synthesis

DHA(L) was synthesized as described in the previous work.[11] In brief, DHAQ and excess stannous chloride were refluxed for 7 h in concentrated hydrochloric acid. The resulting solution was cooled to room temperature, and the precipitate was collected by vaccum filtration. The collected solid was washed with DI water then dried *in vacuo* to afford pale yellow powder.

Anthrone-2,7-disulfonic acid (ADS) was synthesized by following the similar procedure. Anthraquinone-2,7-disulfonate sodium (4.12 g, 10.0 mmol) and excess stannous chloride (9.50 g, 50.0 mmol) in 1 M hydrochloric acid aqueous solution were heated at 80 °C for 24 h. The resulting solution was cooled to room temperature, and the precipitate was collected by vacuum filtration. The solid was dried *in vacuo* to afford pale yellow powder. Under nitrogen protection, the powder was then dissolved in 1 M HCl and subject to ion-exchange column to obtain anthrone-2,7-disulfonic aid (ADS), the solution was condensed by rotavap and dried *in vacuo* to afford the product (90%).

Anthraquinone-2,7-disulfonate sodium was purchased from ASTATech and ion exchanged to anthraquinone-2,7-disulfonic acid.

Characterization

Ex situ ^{1}H NMR spectra were recorded on Varian INOVA 500 spectrometers at 500 MHz. Aliquots were taken and put into deuterated water (D_2O), corresponding NMR spectra were recorded in D_2O with the residual H_2O (δ 4.79 ppm for ^{1}H NMR). LC−MS was conducted on a Bruker microTOF-Q II mass spectrometer. The sample was diluted by water/acetonitrile (V/V = 1:1) to the desired concentration (~20 μM) before LC−MS measurements.

References:

1. B. T. Huskinson, M. P. Marshak, C. Suh, S. Er, M. R. Gerhardt, C. J. Galvin, X. Chen, A. Aspuru-Guzik, R. G. Gordon and M. J. Aziz, Nature, 2014, 505, 195–198.
2. K. Lin, Q. Chen, M. R. Gerhardt, L. Tong, S. B. Kim, L. Eisenach, A. W. Valle, D. Hardee, R. G. Gordon, M. J. Aziz and M. P. Marshak, Science, 2015, 349, 1529–1532.
3. D. G. Kwabi, Y. Ji and M. J. Aziz, Chem. Rev., 2020, 120, 6467–6489.
4. E. S. Beh, D. De Porcellinis, R. L. Gracia, K. T. Xia, R. G. Gordon and M. J. Aziz, ACS Energy Lett., 2017, 2, 639–644.
5. D. G. Kwabi, K. Lin, Y. Ji, E. F. Kerr, M.-A. Goulet, D. De Porcellinis, D. P. Tabor, D. A. Pollack, A. Aspuru-Guzik, R. G. Gordon and M. J. Aziz, Joule, 2018, 2, 1907–1908.
6. Y. Ji, M. A. Goulet, D. A. Pollack, D. G. Kwabi, S. Jin, D. Porcellinis, E. F. Kerr, R. G. Gordon and M. J. Aziz, Adv. Energy Mater., 2019, 9, 1900039.
7. M. Wu, Y. Jing, A. A. Wong, E. M. Fell, S. Jin, Z. Tang, R. G. Gordon and M. J. Aziz, Chem, 2020, 6, 1432–1442.
8. S. Jin, E. M. Fell, L. Vina-Lopez, Y. Jing, P. W. Michalak, R. G. Gordon and M. J. Aziz, Adv. Energy Mater., 2020, 10, 2000100.
9. S. Pang, X. Wang, P. Wang and Y. Ji, Angew. Chem. Int. Ed., 2021, 60, 5289–5298.
10. T. D. Gregory, M. L. Perry and P. Albertus, J. Power Sources, 2021, 499, 229965.
11. M.-A. Goulet, L. Tong, D. A. Pollack, D. P. Tabor, S. A. Odom, A. Aspuru-Guzik, E. E. Kwan, R. G. Gordon and M. J. Aziz, J. Am. Chem. Soc., 2019, 141, 8014–8019.
12. E. W. Zhao, T. Liu, E. Jónsson, J. Lee, I. Temprano, R. B. Jethwa, A. Wang, H. Smith, J. Carretero-Gonzalez, Q. Song and C. P. Grey, Nature, 2020, 579, 224–228.
13. E. W. Zhao, E. Jónsson, R. B. Jethwa, D. Hey, D. Lyu, A. Brookfield, P. A. A. Klusener, D. Collison and C. P. Grey, J. Am. Chem. Soc., 2021, 143, 1885–1895.
14. Y. Jing, M. Wu, A. A. Wong, E. M. Fell, S. Jin, D. A. Pollack, E. F. Kerr, R. G. Gordon and M. J. Aziz, Green Chem., 2020, 22, 6084–6092.
15. V. Y. Fain, B. E. Zaitsev and M. A. Ryabov, Russ. J. Org. Chem., 2007, 43, 1460–1465.
16. V. Dieterich, J. D. Milshtein, J. L. Barton, T. J. Carney, R. M. Darling and F. R. Brushett, Transl. Mater. Res., 2018, 5, 034001.
17. M.-A. Goulet and M. J. Aziz, J. Electrochem. Soc., 2018, 165, A1466–A1477.
18. F. Wang, H. Sheng, W. Li, J. B. Gerken, S. Jin and S. S. Stahl, ACS Energy Lett., 2021, 6, 1533–1539.
19. A. A. Shaw, C. Salaun, J.-F. Dauphin, A. Bernard, J. Magn. Reson., Series A, 1996, 120, 6, 110–115.